UV resonance Raman studies of peptide conformation in poly(L-lysine), poly(L-glutamic acid), and model complexes: the basis for protein secondary structure determination

ARTICLE *in* JOURNAL OF THE AMERICAN CHEMICAL SOCIETY · JUNE 1989

Impact Factor: 12.11 · DOI: 10.1021/ja00194a022

2 AUTHORS, INCLUDING:

Sanford A Asher
University of Pittsburgh
312 PUBLICATIONS **13,133** CITATIONS

SEE PROFILE

UV Resonance Raman Studies of Peptide Conformation in Poly(L-lysine), Poly(L-glutamic acid), and Model Complexes: The Basis for Protein Secondary Structure Determinations

Sunho Song and Sanford A. Asher*

Contribution from the Department of Chemistry, University of Pittsburgh, Pittsburgh, Pennsylvania 15260. *Received October 27, 1988*

Abstract: We have examined the UV Raman spectra of a series of amino acids, dipeptides, tripeptides, and the polypeptides poly(L-glutamic acid) and poly(L-lysine) in their random coil, α-helical and β-sheet forms. Our study examines the assignments of the resonance-enhanced amide bands and characterizes their resonance enhancement mechanisms. We have for the first time characterized the conformational dependence of the intense newly assigned band that derives from the overtone of the amide V vibration. We have examined the pH and conformational dependence of the amide band frequencies and Raman cross sections and relate these dependences to changes in the resonant electronic transition frequency and oscillator strength. We use these spectral parameters to monitor the thermal conversion of poly(L-glutamic acid) (PGA) and poly(L-lysine) (PLL) from the α-helix to β-sheet form and to determine the pH dependence of the transition of PLL to the β-sheet form. We also demonstrate an α-helix-like intermediate of PGA during the transition to the β-sheet conformation. We propose a quantitative relationship between the observed UV Raman spectral cross sections and frequencies and protein secondary structure that will prove useful for conformational studies. These results will serve as the background for analyses of protein secondary structure.

The recent interest in developing UV resonance Raman spectroscopy (UVRR) as a probe of biological structure and function has centered on characterizing the resonance enhancement mechanisms for amides such as *N*-methylacetamide (NMA)[1-3] and other small model complexes[2,4-7] and for aromatic amino acids[7-12] and some well-characterized proteins.[8,12-17] The results for the amides have demonstrated that the amide II, III, and II′ bands are selectively enhanced by the ca. 190-nm amide $\pi \rightarrow \pi^*$ electronic transition,[2,14] while the amide I band shows less enhancement from this transition but is strongly enhanced by a ca. 160-nm transition.[2] The intensities and frequencies of the amide bands depend upon protein secondary structure due to the conformational dependence of interamide hydrogen bonding interactions and because of the conformational dependence of the amide band normal modes. Further, different peptide conformations show different interamide excitonic interactions that result in hypochromic and hyperchromic alterations for the amide electronic absorption band oscillator strengths. More recently we also demonstrated strong enhancement of the overtone band of the amide V vibration (amide 2V), which is anomalously enhanced due to the twisting of the amide group upon excitation into its π^* excited state.[4,5] Although the fundamental is almost Raman forbidden, the overtone is intense and uniquely sensitive to protein secondary structure.[4,5]

The amide bands can be selectively enhanced in proteins with excitation below 220 nm since the aromatic amino acid Raman cross sections rapidly decrease for excitation below 220 nm, while the amide band cross sections increase. To establish the basis for using the amide band frequencies and Raman cross sections to report on protein secondary structure, we have systematically examined the UV Raman spectra of a series of small model compounds, amino acids, dipeptides, tripeptides, and polypeptides such as poly(L-glutamic acid) (PGA) and poly(L-lysine) (PLL) in their random coil, α-helix, and β-sheet conformations. The random coil, α-helix, and β-sheet structures in PLL and PGA are known to adopt secondary structures similar to those found in proteins.[18-32]

Our study examines the assignment of the resonance-enhanced amide bands and characterizes the enhancement mechanisms. We have, for the first time, characterized the conformational dependence of the newly assigned[4,5] intense amide V overtone band. We have examined the pH and conformational dependence of the amide band vibrational frequencies and Raman cross sections and relate these dependences to the conformational dependence of the frequencies and oscillator strengths of the resonant electronic transition. We monitor the pH and thermal conversions of PLL and PGA between the random coil and α-helix and β-sheet conformations. We derive quantitative relationships between the observed UV Raman spectral frequencies and cross sections and the peptide secondary structure. These results will serve as the background for the analyses of the secondary structure of proteins.

* To whom correspondence should be addressed.

(1) Asher, S. A. *Ann. Rev. Phys. Chem.* **1988**, *39*, 537.
(2) Dudik, J. M.; Johnson, C. R.; Asher, S. A. *J. Phys. Chem.* **1985**, *89*, 3805.
(3) Mayne, L. C.; Ziegler, L. D.; Hudson, B. *J. Phys. Chem.* **1985**, *89*, 3395.
(4) Song, S.; Asher, S. A.; Krimm, S.; Bandekar, J. *J. Am. Chem. Soc.* **1988**, *110*, 8547.
(5) Krimm, S.; Song, S.; Asher, S. A. *J. Am. Chem. Soc.*, previous article in this issue.
(6) Mayne, L. C.; Hudson, B. *J. Phys. Chem.* **1987**, *91*, 4438.
(7) Hudson, B.; Mayne, L. C. *Biological Applications of Raman Spectroscopy*; Spiro, T. G., Ed.; Wiley: New York, 1987; p 181.
(8) Johnson, C. R.; Ludwig, M.; O'Donnell, S.; Asher, S. A. *J. Am. Chem. Soc.* **1984**, *106*, 5008.
(9) Asher, S. A.; Ludwig, M.; Johnson, C. R. *J. Am. Chem. Soc.* **1986**, *108*, 3186.
(10) Ludwig, M.; Asher, S. A. *J. Am. Chem. Soc.* **1988**, *110*, 1005.
(11) Johnson, C. R.; Ludwig, M.; Asher, S. A. *J. Am. Chem. Soc.* **1986**, *108*, 905.
(12) Rava, R. P.; Spiro, T. G. *J. Phys. Chem.* **1985**, *89*, 1856.
(13) Copeland, R. A.; Spiro, T. G. *J. Am. Chem. Soc.* **1986**, *108*, 1281.
(14) Copeland, R. A.; Spiro, T. G. *Biochemistry* **1987**, *26*, 2134.
(15) Fodor, S. P. A.; Spiro, T. G. *J. Am. Chem. Soc.* **1986**, *108*, 3198.
(16) Rava, R. P.; Spiro, T. G. *Biochemistry* **1985**, *24*, 1861.
(17) Copeland, R. A.; Spiro, T. G. *Biochemistry* **1985**, *24*, 4960.
(18) Yasui, S. C.; Keiderling, T. A. *J. Am. Chem. Soc.* **1986**, *108*, 5576.
(19) Paterlini, M. G.; Freedman, T. B.; Nafie, L. A. *Biopolymers* **1986**, *25*, 1751.
(20) Davidson, B.; Fasman, G. D. *Biochemistry* **1967**, *6*, 1616.
(21) Gill, Jr., T. J.; Ladoulis, C. T.; Kunz, H. W.; King, M. F. *Biochemistry* **1972**, *11*, 264.
(22) Grourke, M. T.; Gibbs, J. H. *Biopolymers* **1971**, *10*, 795.
(23) Rosenheck, K.; Doty, P. *Proc. Natl. Acad. Sci. U.S.A.* **1961**, *47*, 1775.
(24) Itoh, K.; Foxman, B. M.; Fasman, G. D. *Biopolymers* **1976**, *15*, 419.
(25) Fasman, G. D.; Itoh, K.; Liu, C. S.; Lord, R. C. *Biopolymers* **1978**, *17*, 1729.
(26) Koenig, J. L.; Frusour, B. *Biopolymers* **1972**, *11*, 1871.
(27) Painter, P. C.; Koenig, J. L. *Biopolymers* **1976**, *15*, 229.
(28) Yu, T.; Lippert, J. L.; Peticolas, W. L. *Biopolymers* **1973**, *12*, 2161.
(29) Sengupta, P. K.; Krimm, S. *Biopolymers* **1985**, *24*, 1479.
(30) Sengupta, P. K.; Krimm, S.; Hsu, S. L. *Biopolymers* **1984**, *23*, 1565.
(31) Sugawara, Y.; Harada, I.; Matsura, H.; Shimanouchi, T. *Biopolymers* **1978**, *17*, 1405.
(32) Chinsky, L.; Jolles, B.; Laigle, A.; Turpin, P. Y. *J. Raman Spectrosc.* **1985**, *16*, 235.

0002-7863/89/1511-4295$01.50/0

Experimental Section

The amino acid monomers, dimers, and the polypeptides were obtained from Sigma Chemical Co. (St. Louis, MO) and were, unless specified, used without further purification. Glycylglycine methyl ester was prepared according to known procedures.[33] The identity and purity of the reaction products were confirmed by ^1H NMR, ^{13}C NMR, and elemental analysis. The PGA used was in the form of the sodium salt and had a molecular weight of 26 500 D. The PLL samples, which were obtained as the bromide salt with a molecular weight of 22 000 D, were converted to the chloride salt by extensive dialysis against 0.5 N HCl followed by extensive dialysis against water. D_2O (99.8%) was obtained from ICN Biochemical Inc. (Cambridge, MA). The polypeptides were deuterated by repeated dissolution and incubation for 24 h in D_2O at room temperature, followed by lyophilization. The small peptides were deuterated by simply being dissolved in D_2O. The pD values were obtained from pH electrode measurements corrected by using the method of Glasoe and Long.[34] The samples were titrated by addition of 0.1 N HCl and NaOH for the H_2O solutions and by addition of DCl and NaOD for the D_2O solutions. Each sample contained 0.2 M sodium perchlorate as an internal intensity standard.

The Raman spectra of the solutions were measured in a flowing recirculating stream in which the sample solutions were pumped through a 1-mm i.d. Suprasil quartz capillary by a peristaltic pump. The sampling optics used a 135° backscattering geometry. The Raman instrumentation is described in detail elsewhere.[35] The sample solutions (10–25 mL) were irradiated for ca. 15 min by using pulse energy fluxes between 12 and 79 mJ/(cm^2·pulse) at pulse repetition rates of 20 Hz. The Raman cross sections derive from measured peak-height ratios between the amide bands and those of the internal standard or the D_2O band and from our measured internal standard Raman cross sections.[36] Absorption spectra were measured before and after the Raman spectral measurements to ensure that no irreversible photochemical alterations occurred during the laser illumination. The absorption spectra were measured with a Super Scan UV–vis spectrophotometer, Model 3 (Varian Tech., Pty Ltd., Springvale, Australia). The shorter wavelength (<200 nm) UV absorption spectra were biased by the spectrometer stray light. We corrected the spectral data by an independent measurement of the stray light bias of the spectrometer.

PGA and PLL sample concentrations of 3 mg/mL were used for the spectra excited at 218 nm. Higher concentrations were used for excitation at longer wavelengths. The solutions containing the α-helical form of PGA (pH < 5, room temperature) showed no aggregation or precipitation. The β form of PGA was obtained by heating PGA solutions (pH = 4.3 or pD = 4.1) to 95 °C for 5 days. Fasman and co-workers[24,25] earlier demonstrated the formation of two different β forms of PGA. The species formed depended upon sample concentration and temperature. They observed a rapid formation of the β_1 form at 40–85 °C but at longer times observed formation of another antiparallel β-pleated sheet conformation (β_2 form) for highly concentrated solutions at temperature above 85 °C. However, in our studies, we find that samples, kept at pH = 4.3 at 80 °C for 3.5 days, exist in a state that appears intermediate between the α-helix and the β form of PGA (vide infra).

We observe much slower formation kinetics for the β form and find no evidence for formation of two β forms. Further, we observe aggregation and gel formation prior to any Raman spectral changes diagnostic of formation of the β form. The slower conversion to the β form for our samples may be due to the fact that our samples are more dilute than those studied by Fasman et al.[24] that showed facile formation of both the β_1 and β_2 conformation. This possibility is consistent with the Fasman et al. circular dichroism observation that the rate of the thermal conversion to the antiparallel β conformation decreases at lower PGA concentrations.[24]

Results

Figure 1 shows the UV absorption spectra of aqueous PLL solutions in which the peptide occurs in the α-helical, β-sheet, and random coil conformations. Also shown is an orbital energy level diagram[37] that summarizes the assignments of these electronic transitions to either $\pi \rightarrow \pi^*$ or $n \rightarrow \pi^*$ orbital excitations. The 191-nm $\pi \rightarrow \pi^*$ absorption bands of the α-helical and random coil conformations shift to 193.5 nm in the β-sheet conformation.

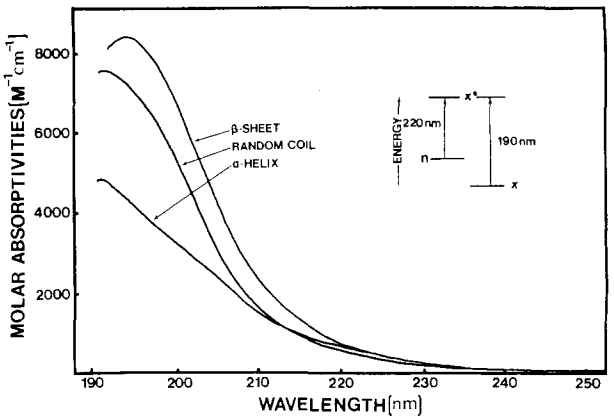

Figure 1. UV absorption spectra of aqueous solutions of poly(L-lysine) and an energy level diagram showing the electronic transitions.[37] β-sheet, pH = 11.2, 52 °C. Random coil, pH = 4.1, 25 °C. α-helix, pH = 11.0, 25 °C.

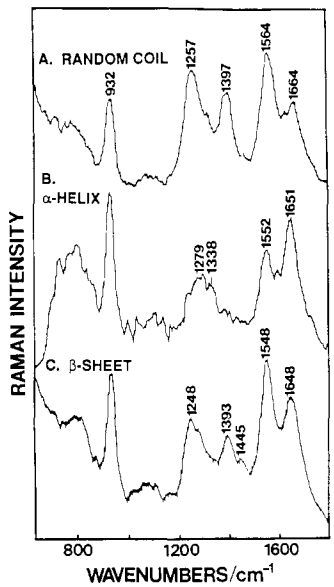

Figure 2. Raman spectra of PGA (0.11 mM) in water at 218-nm excitation, with $NaClO_4$ (0.2 M). The 932-cm^{-1} band derives from ClO_4^- stretching: (A) random coil form, pH = 10.0, 25 °C; (B) α-helix form, pH = 4.3, 25 °C; (C) β-sheet form, pH = 4.3, 95 °C.

The random coil conformation shows a maximum molar absorptivity of 7700 M^{-1} cm^{-1} per peptide linkage. A ca. 10% increased molar absorptivity is evident for the β-sheet conformation relative to that of the random coil form, while the conformational change from the random coil to the α-helical form results in hypochromism for the 191-nm absorption band due to alterations in the proximities and orientations of the amide $\pi \rightarrow \pi^*$ electronic transition moments; the molar absorptivity decreases to 4900 M^{-1} cm^{-1}. The peptide conformational differences result in alterations in amide group excitonic interactions that cause hypochromism for the 191-nm band but cause hyperchromism for the ca. 160-nm band (not shown).[37-40] The α-helical conformation also shows a shoulder at ca. 205 nm, which derives from exciton resonance splitting.[41] The absorption spectrum of random coil and α-helix PGA shows a similar dependence upon conformation (not shown). We were unable to measure absorption spectra of PGA β-sheet conformation because of the high concentration requirement for

(33) Boreham, C. J.; Buckingham, D. A.; Keene, F. R. *Inorg. Chem.* **1979**, *18*, 28.
(34) Glasoe, P. K.; Long, F. A. *J. Phys. Chem.* **1960**, *64*, 188.
(35) Asher, S. A.; Johnson, C. R.; Murtaugh, J. *Rev. Sci. Instrum.* **1983**, *54*, 1657.
(36) Dudik, J.; Johnson, C. R.; Asher, S. A. *J. Chem. Phys.* **1985**, *82*, 1732.
(37) Gratzer, W. B. *Poly-α-Amino Acids, Models for Conformational Studies*; Fasman, G. D., Ed.; Marcel Dekker: New York, 1967; Chapter 5.
(38) Robin M. B. *Higher Excited States of Polyatomic Molecules*; Academic Press: New York, 1975; Vol. II, p 140.
(39) Momii, R. K.; Urry, D. W. *Macromolecules* **1968**, *1*, 372.
(40) Onari, S. *Jpn. J. Appl. Phys.* **1970**, *9*, 227.
(41) Moffitt, W. *Proc. Natl. Acad. Sci. U.S.A.* **1956**, *42*, 736.

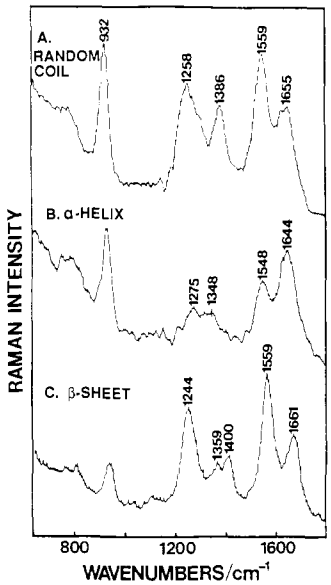

Figure 3. Raman spectra of PLL (0.17 mM) in water at 218-nm excitation, with $NaClO_4$ (0.2 M). The 932-cm^{-1} band derives from ClO_4^- stretching: (A) random coil form, pH = 4.0, 25 °C; (B) α-helix form, pH = 11.0, 25 °C; (C) β-sheet form, pH = 11.3, 52 °C.

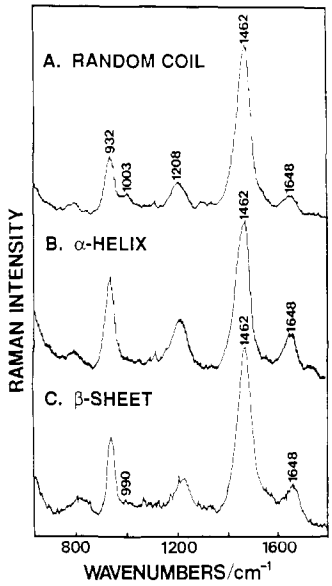

Figure 4. Raman spectra of PGA (0.11 mM) in D_2O with 218-nm excitation with $NaClO_4$ (0.2 M): (A) random coil form, pD = 10.0, 25 °C; (B) α-helix form, pD = 4.5, 25 °C; (C) β-sheet form, pD = 4.1, 95 °C.

β-sheet formation and because of the gel formation that occurs. The maximum molar absorptivities of PGA in the α-helix and the random coil conformations are 4600 and 8000 M^{-1} cm^{-1}, respectively.

Figures 2 and 3 show UV Raman spectra obtained with excitation at 218 nm for different conformations of PGA and PLL in H_2O, while Figures 4 and 5 show spectra obtained for PGA and PLL dissolved in D_2O. The 932-cm^{-1} bands in the spectra derive from sodium perchlorate added to each sample as an internal intensity standard. The Raman spectra of PGA and PLL dissolved in H_2O are dominated by intense bands at ca. 1650 (amide I), 1550 (amide II), and 1250 cm^{-1} (amide III), which have previously been well characterized in terms of their vibrational potential energy distributions.[2,3,42,43] The intensity patterns are

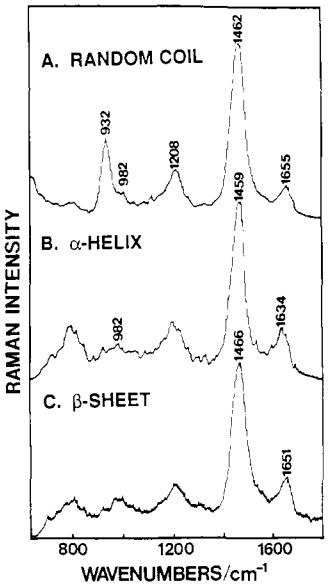

Figure 5. Raman spectra of PLL (0.17 mM) in D_2O with 218-nm excitation with $NaClO_4$ (0.2 M): (A) random coil form, pD = 4.0, 25 °C; (B) α-helix pD = 11.3, 25 °C; (C) β-sheet form, pD = 11.3, 52 °C.

reminiscent of those we observed earlier in the 240-nm excited Raman studies of *N*-methylacetamide (NMA).[2] The peptide conformational frequency dependences for the amide I and amide III bands have previously been characterized by numerous visible wavelength Raman and IR studies of peptides and proteins.[42-44] In addition to the amide modes we also observe prominent bands at ca. 1400 cm^{-1} in the random coil and the β-sheet conformations of PGA and PLL, which can be assigned[4,5] to overtone bands of the amide V vibrations (amide 2V).

Raman spectra of PGA and PLL dissolved in D_2O dramatically differ from those observed in H_2O solution because the increase in the mass of the deuterium atom exchanged for the amide hydrogen dramatically alters the vibrational normal mode distribution. The resulting amide II′ vibration dominates the UV Raman spectra of peptides[3,31] and proteins[13,17] dissolved in D_2O. The amide II vibration (CONH) which occurs at ca. 1550 cm^{-1} is dominated by C–N stretching and N–H in-plane bending.[2,3,42,43] In contrast the amide II′ (COND) vibration which shifts down by 100 cm^{-1} to ca. 1460 cm^{-1} is almost a pure C–N stretch.[3,43] The amide I′ band observed in D_2O solution is relatively weak and shifted to slightly lower frequency at ca. 1650 cm^{-1}. Tables I and II list the Raman band frequencies and cross sections with 218- and 245-nm excitation for the different conformations of PGA and PLL in both H_2O and D_2O solution.

Our previous Raman measurements of NMA excited between 217 and 560 nm clearly indicate that preresonance enhancements of the amide II and III bands of NMA (that are dominated by C–N stretching and CN–H in-plane bending[2,42,43]) derive primarily from the ca. 190-nm $\pi \rightarrow \pi^*$ transition.[2] The amide II and III Raman cross sections of PGA and PLL (Tables I and II) increase similarly for an excitation wavelength decrease from 245 to 218 nm. For NMA the amide I band, which derives primarily from C=O stretching,[2,42,43] is not as strongly enhanced by the ca. 190-nm $\pi \rightarrow \pi^*$ transition; thus, a smaller cross section increase occurs for 218-nm compared to 245-nm excitation.

The 1400-cm^{-1} amide 2V band, which is strongly enhanced for PGA and PLL samples, in the random coil and β-sheet conformations shows a cross section increase between 245- and 218-nm excitation similar to that of the amide II and III bands. It should be noted that our assignment of this ca. 1400-cm^{-1} band[4,5] contrasts sharply with the previous assignments of this band to symmetric stretching modes of carboxylate groups ($\nu_{(COO^-)_s}$) or to CH_2 wagging ($(CH_2)_w$).[6,26-32] The amide V vibration contains C–N

(42) Miyazawa, T. *Poly-α-Amino Acids, Models for Conformational Studies*; Fasman, G. D., Ed.; Marcel Dekker: New York, 1967; Chapter 2.
(43) Krimm, S.; Bandekar, J. *Adv. Protein Chem.* **1986**, *38*, 181.
(44) Tu, A. T. *Raman Spectroscopy in Biology: Principles and Applications*; Wiley: New York, 1982; p 65.

Table I. Raman Frequency and Raman Cross Section of PGA in H_2O and in D_2O for 218- and 245-nm Excitation

	α-helix			random coil			β-sheet		
amide assgnt	freq[a]	σ_{218}[b]	σ_{245}[b]	freq[a]	σ_{218}[b]	σ_{245}[b]	freq[a]	σ_{218}[b]	σ_{245}[b]
				H_2O					
I	1651	3.1	0.23	1664	5.1	0.24	1648	3.8	0.21
II	1552	3.4	0.14	1564	10	0.29	1548	6.9	0.26
III	1279	3.2	0.13	1257	11	0.31	1248	5.7	0.27
2V	1338	2.5	0.10	1397	8.3	0.28	1393	4.4	0.27
							1445		
				D_2O					
I′	1648	2.7	0.14	1648	1.8	0.11	1648	3.0	0.37
II′	1462	11	0.49	1462	20	0.56	1462	15	1.4
III′				1003			990		

[a] Unit: cm^{-1}. [b] Unit: mbarn/(molecule·sr).

Table II. Raman Frequency and Raman Cross Section of PLL in H_2O and in D_2O for 218- and 245-nm Excitation

	α-helix			random coil			β-sheet		
amide assgnt	freq[a]	σ_{218}[b]	σ_{245}[b]	freq[a]	σ_{218}[b]	σ_{245}[b]	freq[a]	σ_{218}[b]	σ_{245}[b]
				H_2O					
I	1644	3.4	0.32	1655	3.7	0.22	1661	9.3	0.46
II	1548	3.7	0.16	1559	8.5	0.23	1559	19	0.33
III	1275	3.3	0.17	1258	8.1	0.31	1244	17	0.41
2V	1348	2.7	0.13	1386	6.0	0.18	1400	8.3	0.14
							1359		
				D_2O					
I′	1634	3.0	0.30	1655	2.5	0.24	1651	4.9	0.31
II′	1459	13	0.39	1462	16	0.50	1466	21	0.49
III′	982			982					

[a] Unit: cm^{-1}. [b] Unit: mbarn/(molecule·sr).

torsion and N–H out-of-plane bending[29,30] and as a fundamental is expected to be weak (vide infra). The overtone is fully allowed and is enhanced due to the geometry alterations between electronic ground and excited states.[4,5]

Frequency changes occur for the amide I, II, III, and 2V bands of PGA and PLL as the conformational changes between random coil, α-helix, and β-pleated sheet. For PGA and PLL the α-helix to the random coil transition occurs if the pH is changed to a value where the side chain becomes charged; PGA forms a random coil or unordered structure[45,46] at high pH, and PLL forms a random coil or unordered form[45,46] at low pH. The amide I, II, 2V, and III bands of the random coil conformation of PGA (PLL) occur at 1664, 1564, 1397, and 1257 cm^{-1} (1655, 1559, 1386, and 1258 cm^{-1}).

Because of the strong intramolecular hydrogen bonding and the unique coiling in the α-helical conformation, the amide I, II, and III bands of α-helical PGA (PLL) occur at 1651, 1552, and 1279 cm^{-1} (1644, 1548, and 1275 cm^{-1}), respectively. The amide 2V band appears to be responsible for the feature at 1338 cm^{-1} for PGA and 1348 cm^{-1} for PLL.[4,5] The amide III bands of the α-helix conformations of both PGA and PLL appear very broad, due to their decreased relative intensities and their overlap with the amide 2V bands. The increased bandwidth could also partially derive from an increase in distribution of peptide conformations or from changes in the amide III vibrational normal mode distribution that result from alterations in the coupling between the amide III and amide 2V vibrations.

A transformation to the β-sheet can be thermally induced by heating α-helical samples. Davidson and Fasman proposed that transformation from an α-helix to β-sheet structure for PLL occurs through a random coil intermediate.[20] The Figure 6 Raman spectra of PLL at 52 °C show the pH dependence of the evolution from the α-helix conformation to the β-sheet. The Raman spectrum in Figure 6A is typical of α-helical PLL below room temperature at pH values between 10.6 and 11.3. Only small frequency and intensity changes are observed as the pH increases to 11.3 for samples maintained at room temperature or 0 °C.

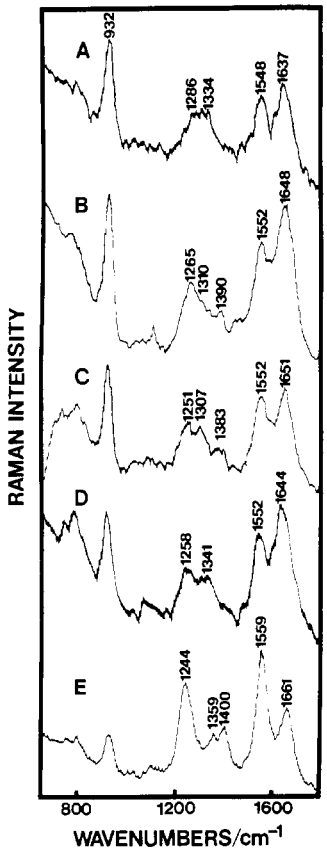

Figure 6. Raman spectra of α-helical PLL, and its dependence upon pH at 52 °C: (A) α-helix conformation, pH = 10.6 at 0 °C; (B) pH = 10.6 at 52 °C; (C) pH = 10.8 at 52 °C; (D) pH = 11.0 at 52 °C; (E) pH = 11.3 at 52 °C. All samples contain 0.2 M $NaClO_4$.

Figure 6B–E shows spectra of PLL at 52 °C at pH values between 10.6 and 11.3. The pH < 11 spectra show an amide I intensity greater than that of amide II (without subtraction of the over-

(45) Sengupta, P. K.; Krimm, S. *Biopolymers* **1987**, *26*, S99.
(46) Tiffany, M. L.; Krimm, S. *Biopolymers* **1968**, *6*, 1379.

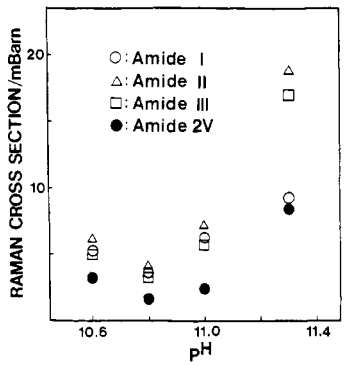

Figure 7. pH dependence of the Raman cross sections of the amide bands of PLL at 52 °C (excitation at 218 nm). Amide I (○), amide II (△), amide III (□), and the overtone of amide V (●). The amide V overtone cross sections shown derive from intensity measurements at ca. 1390 cm^{-1}.

lapping water band). The amide III band appears very broad due to overlap with the amide 2V band. In contrast, the pH 11.3 spectrum (6E) shows a stronger amide II than amide I band, a strong narrow amide III band, and an amide 2V band shifted up to 1400 cm^{-1}. In addition, we assign the new weak 1359-cm^{-1} band to amide 2V vibration (vide infra). The amide I and II bands of PLL (at pH values below pH = 11.0) located at 1648 and 1552 cm^{-1} increase to 1661 and 1559 cm^{-1}, while the 1251–1265-cm^{-1} amide III band downshifts to 1244 cm^{-1} in the pH = 11.3 sample.

Figure 7 illustrates the pH dependence of the Raman cross sections of PLL amide bands at 52 °C. The Raman cross sections of all the bands show a minimum at pH 10.8 with cross sections approximately half of those found at pH 11.3. PLL occurs in a random coil conformation at room temperature and low pH values; a random coil to an α-helix conformational transition occurs as the pH increases. The minimum in the cross section at pH = 10.8 indicates a maximum in the α-helical peptide concentration. Indeed, the amide I, II, and III observed Raman cross sections in the pH = 10.8 sample are close to those for the α-helix conformation. The Raman cross section increase at pH values above 10.8 is associated with an increasing β-sheet content. The β-sheet conformation dominates at pH values greater than 11. These data suggest that the α-helix to β-sheet transition occurs only at pH values greater than 11. This value is one pH unit higher than that observed by Gill et al.[21] The Raman spectra of β-sheet PLL measured at pH = 11.3 and 52 °C show amide I, II, 2V, and III bands at 1661, 1559, 1400 and 1359, and 1244 cm^{-1}, respectively (Figures 3 and 6).

The conversion of α-helical PGA to the β-sheet causes the amide I and II bands to decrease from 1651 and 1552 cm^{-1} to 1648 and 1548 cm^{-1}, respectively. The amide III band decreases more dramatically from 1279 to 1248 cm^{-1}. The intensity of the amide II band becomes larger than amide I. The new bands at 1445 and 1393 cm^{-1} are easily assigned[5] to the overtone of the amide V vibration in view of the Sengupta et al.[30] earlier prediction for amide V band splitting in the β-sheet conformation of PGA. We assume that the 1359-cm^{-1} band in β-sheet PLL derives from a similar splitting.

The different conformations of PGA and PLL in D_2O solutions show smaller Raman frequency and intensity differences. Random coil PLL amide I′ and II′ bands (Figure 5) at 1655 and 1462 cm^{-1} shift down to 1634 and 1459 cm^{-1} in the α-helical conformation but shift back up in the β-sheet form to 1651 and 1466 cm^{-1}, close to those of the random coil conformation. For PGA the random coil amide I′ and II′ bands (Figure 4) that occur at 1648 and 1462 cm^{-1} do not appear to shift in response to those solution temperature and pH changes that should result in formation of the α-helical and β sheet forms. However, changes are observed in the Raman cross sections of these bands (vide infra).

The Raman cross sections of the amide II, III, and 2V bands strongly depend upon conformation (Table I and II) because of the strong hypochromism of the preresonant ca. 190-nm $\pi \rightarrow \pi^*$ transition in the α-helix and the hyperchromism and red shift shown for the β-sheet conformation. For example, the PLL amide II band cross section for 218-nm excitation, which shows a maximum of 19 mbarn in the β-sheet form, decreases to 8.5 and 3.7 mbarn in the random coil and α-helical forms, respectively. The increased cross section of the β-sheet conformation probably results from the red shift of its absorption band towards the 218-nm excitation wavelength (Figure 1). The amide III band cross section shows a similar conformational dependence. The similar cross sections of the amide II and III bands are a consequence of their similar potential energy distributions. The amide 2V band also shows a similar cross-section dependence with a value of 6.0 mbarn per peptide linkage for the random coil conformation. This decreases to 2.7 mbarn in the α-helix but increases to 8.3 mbarn in the β-sheet conformation. In contrast, the PLL amide I band cross section is less sensitive to conformation; its enhancement has a major contribution from transitions deeper in the UV than the ca. 190-nm $\pi \rightarrow \pi^*$ transition.

For D_2O solutions, the PLL amide II′ band cross section with 218-nm excitation decreases from 21 mbarn in the β-sheet to 16 and 13 mbarn in the random coil and α-helix conformations, respectively. For PGA, a conformational cross-section dependence occurs even though only a meager frequency conformational dependence is observed. The amide II′ band conformational cross section dependence is similar but somewhat less than that observed for the amide II and III bands. For D_2O solutions, the PGA amide II′ cross section is a maximum for the random coil form at 20 mbarn and decreases to 15 and 11 mbarn in the β-sheet and α-helical forms, respectively.

It is interesting that the amide II′ cross sections are always larger than those of the amide II and III bands. This occurs because C–N stretching dominates the enhancement mechanism and a larger component of C–N stretching is present in the amide II′ band compared to that of amide II or III bands.[3,43] In the α-helical form of PGA and PLL the amide II′ cross section is almost twice the sum of that of the amide II and III bands. In the random coil form of PGA and PLL, it is almost equal to the sum of the amide II and III cross sections. In β-sheet PGA the amide II′ cross section is larger than the sum of the amide II and III cross sections. In contrast, the PLL amide II′ cross section in the β-sheet form is only slightly greater than that of the amide II or III band.

The cross section values reported here derive from peak-height measurements and are directly related to the maximum differential Raman cross sections ($d\sigma/d\nu$). If the bandwidths are close to that of the internal standard or are smaller than the spectrometer resolution, the measured maximum differential Raman cross sections are equal to the total (integrated) Raman cross sections. In our measurements we used a ca. 29-cm^{-1} bandpass for the 218-nm spectra. Thus, our peak-height cross sections are essentially identical with the total cross sections. We expect that the maximum differential Raman cross sections are of more utility than integrated cross sections because of the difficulty of resolving overlapping Raman bands, especially when the amide cross sections are small such as for the α-helix form. Futher, because of band overlap we expect that peak-height measurements will be more useful for protein conformational studies. The changes we observe in Raman cross sections may derive partially from inhomogeneous band broadening due to the different distributions of conformations and environments that occur in different peptide conformations. Mayne et al.[3] have recently observed an insidious version of inhomogeneous broadening in their failure to resolve the amide I and I′ bands of NMA in H_2O and D_2O. These bands become readily apparent for NMA in acetonitrile solution, presumably due to the narrowing of the inhomogeneously broadened bandwidth.[3]

We examined a series of model compounds to determine the dependence of the amide band cross sections upon the amide group geometry, upon the nature of the side chain, and upon the effect of the charge state of the peptide terminal end groups. Figure 8 and 9 show the 218-nm excited Raman spectra of the small model complexes glycylglycine (DGL), glycylglycylglycine (TGL), *N*-acetylglycine (AGL), L-alanyl-L-alanine (DLA), L-valyl-L-valine

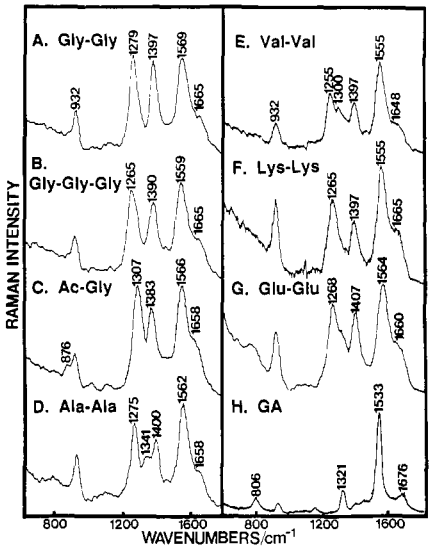

Figure 8. Raman spectra of small peptide model complexes in water with excitation of 218 nm: (A) glycylglycine (DGL) at pH = 4.5; (B) glycylglycylglycine (TGL) at pH = 4.5; (C) *N*-acetylglycine (AGL) at pH = 4.5; (D) L-alanyl-L-alanine (DLA) at pH = 4.5; (E) L-valyl-L-valine (DLV) at pH = 4.5; (F) α-L-lysyl-α-L-lysine (DLL) at pH = 4.0; (G) α-L-glutamyl-α-L-glutamic acid (DLG) at pH = 4.5; (H) 2,5-piperazinedione (GA). All spectra show the 932-cm^{-1} band of ClO_4^- (0.2 M).

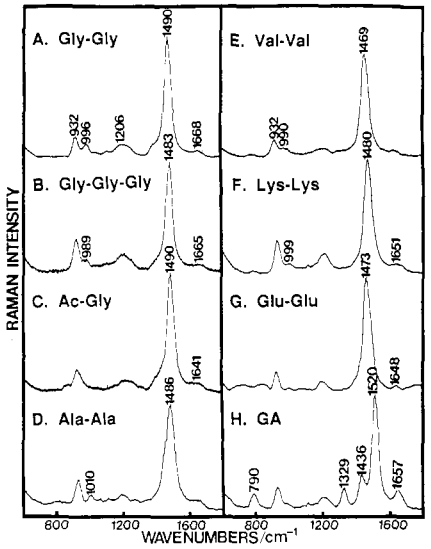

Figure 9. Raman spectra of small peptides in D_2O solution at 218-nm excitation with $NaClO_4$ (0.2 M): (A) glycylglycine (DGL) at pD = 4.5; (b) Glycylglycylglycine (TGL) at pD = 4.5; (C) *N*-acetylglycine (AGL) at pD = 4.5; (D) L-alanyl-L-alanine (DLA) at pD = 4.5; (E) L-valyl-L-valine (DLV) at pD = 4.5; (F) α-L-lysyl-α-L-lysine (DLL) at pD = 4.0; (G) α-L-glutamyl-α-L-glutamic acid (DLG) at pD = 4.5; (H) 2,5-piperazinedione (GA).

(DLV), α-L-lysyl-α-L-lysine (DLL), α-L-glutamyl-α-L-glutamic acid (DLG), and 2,5-piperazinedione (GA) (also known as diketopiperazine or as glycine anhydride) in water and D_2O solution at pH = 4.5 or 4.0. Table III lists the observed Raman band frequencies, the Raman cross sections, and the band assignments. As previously observed for NMA,[2,3] PGA, and PLL, the amide II, III, and II′ bands dominate the UV Raman spectra. Strong enhancement of the overtone of amide V occurs for all the model complexes except for GA. It is difficult to resolve the weak amide I bands of these derivatives, probably because of inhomogeneous broadening due to the hydrogen bonding with water and due to the overlap with the OH bending band of water. Although weak, the amide I′ band is observed in D_2O solution (Figure 9).

The frequencies of the amide II, 2V, III, and II′ bands are sensitive to the nature of the side chain and vary between 1555 and 1569 cm^{-1}, 1383 and 1407 cm^{-1}, 1255 and 1307 cm^{-1}, and 1469 and 1490 cm^{-1} for these derivatives. The cross sections of the amide I bands are relatively constant at ca. 3 mbarn, close to that observed for PGA and PLL. In contrast, the cross sections for the amide II, 2V, and III bands vary between 9.1 and 34 mbarn, 8.1 and 19 mbarn, and 11 and 25 mbarn per peptide linkage, respectively. The TGL amide II and III cross sections per peptide linkage are ca. 40% less than those of DGL, while that of amide 2V cross section is ca. 55% of that of DGL. The amide band Raman frequencies are lowest for DLV and approach most closely the frequencies for the amide II and III bands of PGA and PLL in their different conformations. However, the cross sections of the DLV amide II, III, and 2V bands are much larger

Table III. Raman Frequencies and Raman Cross Sections per Peptide Linkage of Small Peptides in the Solid and in Solution

amide assgnt	solid freq[g]	H_2O freq[g]	H_2O σ_{218}[h]	D_2O freq[g]	D_2O σ_{218}[h]
		DGL (pH 4.5, pD 4.5)			
I	1682[a]	1665	3.9	1668	1.3
	1647[a]				
II	1531[a]	1569	16	1490	34
III	1249[a]	1279	19	996	4.1
2V		1397	18		
		TGL (pH 4.5, pD 4.5)			
I	1665[a]	1665	2.8	1655	0.7
II	1525[a]	1559	10	1483	13
III	1240[a]	1265	11	989	1.4
	1221[a]				
2V		1390	9.5		
		AGL (pH 4.5, pD 4.5)			
I	1710[b]	1658	2.8	1641	0.85
II	1557[b]	1566	9.1	1490	17
III	1303[b]	1307	11		
2V		1383	8.1		
		DLA (pH 4.5, pD 4.5)			
I	1681[c]	1658	2.7		
II	1560[c]	1562	13	1486	25
III	1287[c]	1275	13		
	1265[c]				
2V		1400	9.4		
		DLV (pH 4.5, pD 4.5)			
I	1660[d]	1648	4.9		
II	1551[d]	1555	34	1469	70
III	1253[d]	1255	25		
2V		1397	19		
		DLL (pH 4.0, pD 4.0)			
I		1665	4.2	1651	3.2
II		1555	21	1480	51
III		1265	19		
2V		1397	13		
		DLG (pH 4.5, pD 4.5)			
I	1652[e]	1660	6.8	1648	1.9
II		1564	22	1473	72
III	1246[e]	1268	22		
2V		1407	19		
		GA			
amide I	1664[f]				
	1662[f]				
	1623[f]	1676	1.9	1657	4.0
amide II	1519[f]	1533	11	1520	26
CH_2 bend	1423[f]	1442		1436	8.2
N–H bend	1457[f]	1390			
CH_2 wag	1313[f]	1321	3.6	1329	5.1
ring str	795[f]	806	1.9	790	4.5

[a] Smith, M.; Walton, A. G.; Koenig, J. L. *Biopolymers* **1969**, *8*, 29. [b] Sankaranarayanan, V. N.; Krishinan, R. S. *Ind. J. Pure Appl. Phys.* **1972**, *10*, 378. [c] Sutton, P.; Koenig, J. L. *Biopolymers* **1970**, *9*, 615. [d] Fasman, G. D.; Itoh, K.; Liu, C. S.; Lord, R. C. *Biopolymers* **1978**, *17*, 125. [e] Koenig, J. L.; Frushour, B. *Biopolymers* **1972**, *11*, 1871. [f] Cheam, T. C.; Krimm, S. *Spectrochim. Acta* **1984**, *40A*, 503. [g] Units: cm^{-1}. [h] Units: mbarn/(molecule·sr).

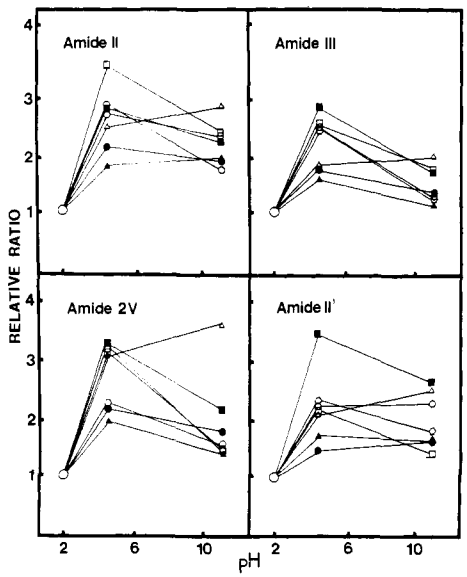

Figure 10. pH dependence of the Raman cross section of the amide II, III, and II′ bands and the overtone band of amide V relative to those at pH = 2: glycylglycine (○), glycylglycylglycine (●), *N*-acetylglycine (△), L-alanyl-L-alanine (▲), L-valyl-L-valine (□), α-L-lysyl-α-L-lysine (◇), and α-L-glutamyl-α-L-glutamic acid (■).

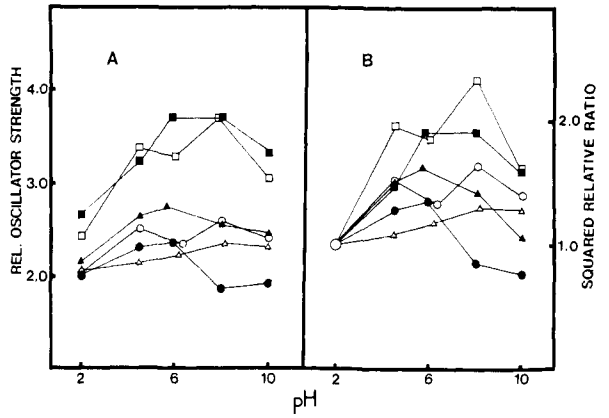

Figure 11. (A) pH dependence of the relative oscillator strength compared to that at pH = 2 calculated from the product of the molar absorptivity and the half-bandwidth of the ca. 190-nm absorption band for glycylglycine (○), glycylglycylglycine (●), *N*-acetylglycine (△), L-alanyl-L-alanine (▲), L-valyl-L-valine (□), and α-L-glutamyl-α-L-glutamic acid (■). (B) pH dependence of the relative value of the square of the oscillator strength compared to that at pH = 2.

than those of polypeptides. The amide III band of AGL cannot be directly compared to the amide bands of the other complexes since this vibration also includes major components of C–CH_3 deformation[47] as does the amide III band of NMA.[2] The Raman cross sections of amide II and III bands of AGL are larger than those of NMA. The amide II′ cross sections for these small model compounds are greater than those of the respective amide II bands. For DGL, AGL, DLV, DLA, DLL, and DLG, the amide II′ band cross section is close to the sum of their amide II and III band cross sections.

The amide 2V bands near 1400 cm^{-1} in these small peptides show Raman cross sections of 8.1–19 mbarn per peptide linkage. These bands occur at frequencies similar to the $\nu_{(COO^-)_s}$ vibrations of acetate ion and carboxylic acids at high pH. However these carboxylate groups show Raman cross sections[5] of only 0.6–0.8 mbarn and thus can contribute little to the intensity of the observed amide 2V band.

Figure 10 illustrates the pH dependence of the cross section for the amide II, III, 2V, and II′ bands. The Raman cross sections in general show a maximum at pH = 4.5 except for AGL, which increases monotonically with increasing pH. Figure 11A shows the pH dependence of the $\pi \rightarrow \pi^*$ band relative oscillator strength obtained by measuring the integrated absorption on the longer wavelength side of the ca. 190-nm absorption band. Figure 11B also shows the pH dependence of the square of the oscillator strength ratio compared to its value at pH = 2. The pH dependence of the Raman cross sections correlates well with the pH dependence of the square of the oscillator strength.

In general, the peptide bonds in proteins and peptides occur in a trans configuration. However, glutamic acid residues at the N terminus can cyclize to form a cis-amide linkage.[44] Cis-amide linkages are also found in small ring lactams.[44] 2,5-Piperazinedione (GA) was used as a model to examine the cis-peptide bond conformation. The cis-peptide model compound, GA, Raman spectrum differs significantly from those of the other peptide complexes that occur in the trans form. Raman spectra of GA (Figures 8H and 9H) show strong bands at 1533, 1321, and 806 cm^{-1} in water and 1657, 1520, 1436, 1329, and 790 cm^{-1} in D_2O. The band at 1442 cm^{-1} is difficult to discern with 218-nm excitation but is clearly observed with 245-nm excitation. Since the GA peptide linkage is constrained in a cis-amide configuration due to the presence of two planar amide groups, the vibrational normal mode composition differs from that of normal unstrained trans-peptides. Essentially pure C–N stretching and N–H bending are observed in the spectra since negligible vibrational coupling between these motions occurs for the cis-peptide configuration.[42] The band frequencies of GA in the solid state are almost identical with those in aqueous solution. Only the 1457-cm^{-1} N–H bending vibration shifts upon dissolution in water to 1390 cm^{-1}.[42,48] This selective shift occurs because N–H bending is very sensitive to the details of intermolecular hydrogen bonding between the GA and water or between GA and GA in the crystal. The fact that this band is very weak with both 218- and 245-nm excitation but is easily observed with 320-nm excitation indicates that the N–H in-plane bending mode is not selectively enhanced by the amide $\pi \rightarrow \pi^*$ transition.

Very similar spectra are observed for GA in H_2O and D_2O. The amide I band, which derives from C=O stretching and ring stretching,[48] which is located at 1676 cm^{-1} in H_2O, shifts to 1657 cm^{-1} in D_2O. This frequency is higher than that in trans-peptides. Cheam and Krimm[48] have shown that the amide II′-like 1533-cm^{-1} band vibrational composition differs dramatically from that of the amide II band of trans-peptides. The 1533-cm^{-1} band is amide II′-like since it contains only a small contribution of N–H bending. In contrast, this vibration in the cis-peptide is dominated by ring stretching and ring deformation, with some C=O stretching and N–H and $-CH_2-$ bending modes.[48] The spectral domination of the cis-amide II band is strikingly similar to the dominance of the amide II′ bands of trans-peptides in D_2O. Upon deuteration, the amide II band of GA shifts only 13 cm^{-1}, in contrast to ca. 100-cm^{-1} shift typical of trans-peptides. This is consistent with the smaller coupling between C–N stretching and N–H bending. The amide III band, which is theoretically predicted[42] to be mainly a C–N stretch of the cis-peptide at 1350 cm^{-1}, is not clearly evident. The strong 1321-cm^{-1} band in this cis-peptide, which derives from $-CH_2-$ wagging,[48] is uniquely enhanced. In addition, a ring stretching mode, arising from C–N stretching and C_α–C stretching,[48] occurs at 1442 and 806 cm^{-1} in water and at 1436 and 790 cm^{-1} in D_2O solution. The amide band Raman cross sections per peptide linkage observed for the cis-peptide GA are lower than those of the trans peptides studied.

Discussion

Raman Band Intensities. The observed Raman cross section dependence upon molecular structure and peptide conformation can be understood in terms of the conventional *A*-term formalism of resonance Raman theory. The total Raman scattering cross section, σ_{mn}, for a vibrational transition n ← m integrated over

(47) Sankaranarayanan, V. N.; Krishinan, P. S. *Ind. J. Pure Appl. Phys.* **1972**, *10*, 378.

(48) Cheam, T. C.; Krimm, S. *Spectrochim. Acta* **1984**, *40A*, 481, 503.

4π sr for an isolated molecule, averaged over all orientations is

$$\sigma_{mn} = I_{mn}/I_0 = (2^7\pi^5/3^2)\nu_0(\nu_0 - \nu_{mn})^3 g f(T) \sum |\alpha_{\rho\sigma}(\nu_0)|^2 \quad (1)$$

I_{mn} is the Raman intensity integrated over 4π sr over the bandwidth of the vibrational transition n ← m. I_0 is the incident laser intensity. ν_0 and ν_{mn} are the excitation and vibrational frequencies, respectively. g is the degeneracy of the initial state, m, and $f(T)$ is the Boltzmann weighting factor describing the thermal occupancy of the initial state. $\alpha_{\rho\sigma}(\nu_0)$ is the ρ,σth component of the Raman polarizability tensor for excitation at ν_0. The polarizability tensor elements can be described by using second-order perturbation theory;[49]

$$\alpha_{\rho\sigma} = \sum_{ev}\left[\frac{\langle gn|\mu_\sigma|ev\rangle\langle ev|\mu_\rho|gm\rangle}{\nu_{ev} - \nu_m - \nu_0 - i\Gamma_e} + \frac{\langle gn|\mu_\rho|ev\rangle\langle ev|\mu_\sigma|gm\rangle}{\nu_{ev} - \nu_n + \nu_0 - i\Gamma_e}\right] \quad (2)$$

where μ_σ and μ_ρ are the electronic dipole moment operators along the molecular coordinates σ and ρ that define the molecular axes with respect to the scattered and incident light polarizations. ν_m and ν_n are the frequencies of the initial and final vibrational states in the ground electronic state $|g\rangle$, and ν_{ev} is the transition frequency to the particular $|ev\rangle$ vibronic state of an excited electronic state $|e\rangle$. Γ_e is a damping factor related to the total dephasing rate of the resonant excited state. The summation is over all excited states except the ground state.

The preresonance frequency dependence of the Raman cross section can be modeled by using the Albrecht A-term expression, which is based on the vibronic theory of the Raman polarizability. The A-term model describes the enhancement mechanism of a totally symmetric mode and assumes the adiabatic approximation. After carrying out the Herzberg–Teller expansion and considering that a single dipole allowed transition dominates eq 2, the preresonance excitation frequency dependence of σ_{mn} is given by[49-51]

$$\sigma_{mn} = K_1\nu_0(\nu_0 - \nu_{mn})^3\left[\frac{\nu_e^2 + \nu_0^2}{(\nu_e^2 - \nu_0^2)^2} + K_2\right]^2 \quad (3)$$

where K_1 and K_2 are constant. K_1 is independent of the excitation frequency and depends on the oscillator strength of the transition and the coupling between the vibration and the electronic transition. K_2 is a phenomenological term that permits the inclusion of an additional preresonant state at very high energy. When $K_2 = 0$, eq 3 corresponds to the simple Albrecht A-term expression.

The Raman cross-section excitation profile data for the amide bands of PGA, PLL, and small peptides between 245- and 218-nm excitation are modeled well by the simple Albrecht A-term expression; Table IV displays the K_1 and ν_e best-fit values. The A-term fits for the amide II, III, and 2V bands for the α-helix and random coil conformations of PGA and PLL indicate preresonant states lying between 193 and 200 nm. These bands for β-sheet PLL show a preresonant state at a somewhat longer wavelength of 200–202 nm, which reflects the 2.5-nm red shift of the $\pi \rightarrow \pi^*$ absorption maximum in the β-sheet conformation. Interestingly, we do not see the same shift for β-sheet PGA. Thus, these data indicate that the amide II, III, and 2V preresonant enhancements derive mainly from the ca. 190-nm $\pi \rightarrow \pi^*$ transition of the peptide linkage. These excitation profile results are consistent with Copeland and Spiro's 192–223-nm resonance Raman study of the random coil conformation of PLL, which demonstrated that the amide II, III, and II′ enhancement derived mainly from the ca. 190-nm $\pi \rightarrow \pi^*$ transition.[14] The A-term fits for DGL, DLG, and DLL also show dominance of the ca. 200-nm amide $\pi \rightarrow \pi^*$ transitions.

The origin of enhancement of the amide II and III bands by the ca. 190-nm $\pi \rightarrow \pi^*$ amide electronic transition was previously deduced to derive from the fact that the amide II and III bands contain a large component of C–N bond stretching. This motion couples to the $\pi \rightarrow \pi^*$ transition since the excited state shows an elongation of the C–N bond compared to that of the ground state. The enhancement of the overtone of amide V occurs because the excited state is also twisted. The amide V vibration is mainly a torsion about C–N bond; the overtone is allowed while the fundamental is "almost" forbidden within the effective "local symmetry".[4,5] A similar selective enhancement of the overtone of the torsional mode occurs for ethylene where the excited state is twisted.[52] This torsional vibration in the D_{2h} point group of ethylene is of A_u symmetry and is strictly Raman forbidden as a fundamental. In the "local" C_{2v} symmetry of the C–N amide linkage the torsion is of A_2 symmetry; while it is not strictly Raman forbidden, it cannot gain intensity from the A-term mechanism and is expected to be extremely weak relative to other symmetric A-term enhanced modes. However, the amide V overtone is of A_1 symmetry. Finally, if we consider the amide linkage to be of C_s symmetry the torsion is of A″ symmetry and is an out-of-plane vibration which as a fundamental is not expected to gain intensity from the in-plane amide $\pi \rightarrow \pi^*$ transition. In addition, as a fundamental it should not be A-term enhanced, but it will be A-term enhanced as an overtone since it is of A′ symmetry.

The preresonant states for amide I band enhancement occur between 178 and 197 nm, at a systematically higher energy than that for the amide II, III, and 2V bands. The amide I vibration is dominated by C=O stretching and will be selectively enhanced by electronic transitions to states with altered C=O bond lengths and force constants. Thus, the amide I band shows a different enhancement pattern than that for the amide II, III, and 2V bands,

Table IV. K_1 and ν_e Values for PGA, PLL, Small Peptides, and Model Complex for $\nu_{(COO^-)_s}$

PGA

amide assgnt	α-helix $10^{-30}K_1$	α-helix ν_e, nm	random coil $10^{-30}K_1$	random coil ν_e, nm	β-sheet[a] $10^{-30}K_1$	β-sheet[a] ν_e, nm
I	5.49	190	18.75	178	3.25	193
II	2.61	196	3.27	197	2.87	198
III	2.46	196	4.35	197	5.58	194
2V	1.97	196	4.95	194	4.48	196

PLL

amide assgnt	α-helix $10^{-30}K_1$	α-helix ν_e, nm	random coil $10^{-30}K_1$	random coil ν_e, nm	β-sheet $10^{-30}K_1$	β-sheet ν_e, nm
I	18.1	184	5.35	192	13.2	192
II	3.44	195	2.76	200	3.29	202
III	4.59	193	5.11	196	5.02	200
2V	3.22	194	2.66	198	1.40	201

amide assgnt	DGL (pH 4.5) $10^{-30}K_1$	DGL (pH 4.5) ν_e, nm	DLL (pH 4.0) $10^{-30}K_1$	DLL (pH 4.0) ν_e, nm	DLG (pH 4.5) $10^{-30}K_1$	DLG (pH 4.5) ν_e, nm
I	3.42	192	11.1	189	4.63	197
II	2.18	203	8.42	199	6.07	201
III	8.97	197	13.2	196	5.97	201
2V	8.67	197	8.05	197	8.57	198

GA

	$10^{-30}K_1$	ν_e, nm
amide I	14.0	182
amide II	30.2	189
ring str	6.98	186

Acetate Ion

	$10^{-30}K_1$	ν_e, nm
$\nu_{(COO^-)_s}$[b]	11.5	173
$(CH_2)_w$[c]	2.82	174

[a] The ν_e data are less reliable for PGA β-sheet since we determined K_1 and ν_e from only two spectra at 245- and 218-nm excitation. [b] Symmetric stretch of carboxylate group. [c] Methylene wag.

(49) Tang, J.; Albrecht, A. C. *Raman Spectroscopy, Theory and Practice*; Szymanski, H. A., Ed.; Plenum: New York, 1970; Vol. II, p 33.
(50) Albrecht, A. C. *J. Chem. Phys.* **1960**, *34*, 1476.
(51) Albrecht, A. C.; Hutley, M. C. *J. Chem. Phys.* **1971**, *55*, 4438.
(52) Ziegler, L. D.; Hudson, B. S. *J. Chem. Phys.* **1983**, *79*, 1197.

which are mainly enhanced by Franck–Condon mechanisms involving C–N bond elongation and π^* excited-state twisting. The higher ν_e value for the amide I band occurs because of a contribution to preresonant enhancement by the ca. 160-nm amide transition. Enhancement of the amide I band by this transition is consistent with its assignment as an $n \rightarrow \sigma^*$ transition, involving promotion of an electron from the 2p orbital of oxygen to an in-phase linear combination of the 3s atomic orbitals of the oxygen, carbon, and nitrogen atoms with the oxygen dominating;[53] this should result in a C=O bond length change. It should be noted, however, that the assignment of the ca. 160-nm transition is controversial and it has also been assigned to a $\pi \rightarrow \pi^*$ transition of the amide group.[37,38]

The cis-peptide amide II′-like band at 1533 cm^{-1} and the ring-stretching mode at 806 cm^{-1} show preresonant states at 189 and 186 nm, respectively. Thus, the enhancement for these bands also derives from the amide $\pi \rightarrow \pi^*$ transition. As observed for trans-peptides, the preresonant state for the amide I band also occurs at a shorter wavelength of 182 nm. Thus, the enhancement of the amide II′-like band derives from the ca. 190-nm $\pi \rightarrow \pi^*$ transition. The preresonant states for the $\nu_{(COO^-)_s}$ and $(CH_2)_w$ vibrations of acetate ion occur at ca. 174 nm.

Conformational Dependence of Raman Cross Sections. The peptide conformational Raman cross section dependence derives directly from the conformational dependence of the absorption spectrum. The oscillator strength of the amide $\pi \rightarrow \pi^*$ transition of polypeptides depends upon excitonic interactions between transition moments of neighboring amide chromophores.[54] The magnitude of excitonic interaction depends intimately on the conformation of polypeptide. Since both the Raman polarizability and oscillator strength are a function of the transition moment, the Raman cross section should be proportional to the square of the oscillator strength (see eq 2) and roughly proportional to the square of the maximum molar absorptivity of the preresonant state. This assumes little change occurs in the vibrational normal-mode distributions and coupling strengths. This appears reasonable in view of the modest changes that occur in vibrational frequencies. Most of these vibrational frequency changes derive from the changes in the peptide coiling geometry. We expect negligible changes in the Raman cross sections due to changes in the dephasing rates as a result of changes in excitonic interactions; these transitions are dominated by inhomogeneous broadening.

The relative Raman cross sections for different polypeptide conformations can, thus, be estimated from the ca. 190-nm $\pi \rightarrow \pi^*$ absorption band molar absorptivities. For PGA the ratio of α-helix to random coil Raman cross sections for excitation at 218 nm are 0.33, 0.31, and 0.30 for the amide II, III, and 2V bands, respectively. For PLL the ratios are 0.44, 0.41, and 0.45 for the amide II, III, and 2V bands, respectively. The predicted α-helix to random coil Raman cross section ratios calculated from the square of the ca. 190-nm molar absorptivities agree reasonably well, at 0.33 and 0.40 for PGA and PLL, respectively. As expected, the amide I cross section ratios of 0.61 and 0.92 for PGA and PLL are less correlated with the ca. 190-nm amide $\pi \rightarrow \pi^*$ molar absorptivity ratio. The amide II′ cross section ratios for PGA and PLL in D_2O of 0.56 and 0.78 are somewhat higher than those of the amide II, III, and 2V bands. All of the results above indicate that the intensities of the amide II, III, 2V, and II′ bands arise from the lowest $\pi \rightarrow \pi^*$ electronic transitions and that the Raman hypochromism observed for the polypeptides derives mainly from the ca. 190-nm UV absorption hypochromism. For 245-nm excitation the ratios of α-helix to random coil Raman cross sections of PGA (PLL) are 0.48, 0.42, 0.36, and 0.88 (0.70, 0.55, 0.73, and 0.78) for the amide II, III, 2V, and II′ bands, respectively. The hypochromism of the 190-nm $\pi \rightarrow \pi^*$ transition affects the Raman cross sections less for excitation far from resonance; the relative contribution of transitions further in the UV increases as excitation occurs further away from resonance with the 190-nm $\pi \rightarrow \pi^*$ transition.

The β-sheet to random coil conformation Raman cross section ratios of PLL at 218-nm excitation are 2.2, 2.1, 1.4, and 1.3 for the amide II, III, 2V, and II′ bands, respectively. A cross section increase of ca. 1.2 would be expected, if only changes in the molar absorptivity are important. The larger ratio observed derives from the red shift of the $\pi \rightarrow \pi^*$ transition in the β-sheet conformation.

Similar cross section increases would be expected for the PGA β-sheet compared to the random coil conformation. Peculiarly, however, lower Raman cross sections occur for the amide II, III, 2V, and II′ bands of PGA in the β-sheet conformation than in the random coil. The PGA Raman cross section ratios of β-sheet to random coil are 0.67, 0.53, 0.53, and 0.75 for the amide II, III, 2V, and II′ bands, respectively. The frequencies of the β-sheet PGA amide I and II band occur at 1648 and 1548 cm^{-1}, ca. 10 cm^{-1} lower than those of the β-sheet conformation of PLL. Interestingly the frequency of the amide I band of PGA β-sheet conformation is identical to that of the β_2 form of PGA observed by Fasman et al.[25] They suggested that the unusually low frequency of the β-sheet amide I band derived from the hydrogen bonding between PGA sidechains.

The differences of the cross-section ratios and the amide band frequencies between PGA and PLL may suggest conformational differences in β-sheet structure between PGA and PLL. PGA may not completely adopt a β-sheet conformation. The driving force for β-sheet formation is strong hydrophobic side-chain interactions.[20] Poly(L-ornithine), which has one less methylene group in the side chain than PLL, does not completely convert to a β-sheet structure.[22] Thus, the shorter side chain of PGA may sufficiently decrease β-sheet stability of PGA to alter the net conformation compared to PLL under our solution conditions. This is consistent with Rosenheck and Doty's UV absorption spectrum of PGA at pH = 3.2 and 90 °C, which shows a β-sheet-like conformation with a molar absorptivity intermediate between that of a random coil and α-helix conformation.[23] This decrease in the molar absorptivity may be responsible for the 2-fold decreased Raman cross section observed.

To summarize, the dramatic Raman cross section differences between β-sheet PGA compared to PLL suggest a radically different β-sheet conformation. Possibly β-sheet PGA shows some similarity to the α-helix structure or the cross section decrease may result from the coexistence of α-helical and β-sheet structure. On the other hand, observation of gel formation, the amide band frequencies, and the splittings of the amide 2V band to 1393 and 1445 cm^{-1} are clearly diagnostic for a PGA β-sheet structure.

The Raman cross sections of the amide bands depend upon the peptide geometry and ionization state. The Raman cross sections per peptide linkage of the small model peptides (Figure 8) are larger than those of PGA and PLL. These increased Raman cross sections of the amide bands may be due to an "end effect" from the terminal end groups.[55] The terminal carboxyl and amino groups cause red shifts for the $\pi \rightarrow \pi^*$ transitions of the terminal peptide linkages compared to those of internal linkages.[37,55] This would directly lead to increased Raman cross sections. Consistent with this, we observe smaller Raman cross sections for N- or C-blocked amino acids such as AGL and glycylglycine methyl ester and ethyl ester (data not shown) compared to those of DGL. Further, the amide cross sections of TGL are 40% lower per peptide segment than those for DGL. For large polypeptides the contribution of the terminal groups must negligibly affect the average amide Raman cross sections.

The Raman cross section maxima observed at pH = 4.5 for all complexes (except for AGL) result from the $\pi \rightarrow \pi^*$ integrated molar absorptivity increase which also occurs at pH = 4.5 (Figures 10 and 11). The monotonic Raman cross section increase for AGL with increasing pH correlates with the monotonic absorption increase. These Raman cross section changes occur in the absence of major frequency shifts for the amide bands. Figure 11B, which shows the dependence of the square of the oscillator strength of the ca. 190-nm absorption band upon pH, resembles Figure 10, which shows the pH dependence of the amide band Raman cross

(53) Peterson, D. L.; Simpson, W. T. *J. Am. Chem. Soc.* **1957**, *79*, 2375.
(54) Tinoco, Jr., I. *J. Am. Chem. Soc.* **1961**, *83*, 3609.
(55) Saidel, L. J. *Arch. Biochem. Biophys.* **1955**, *54*, 184.

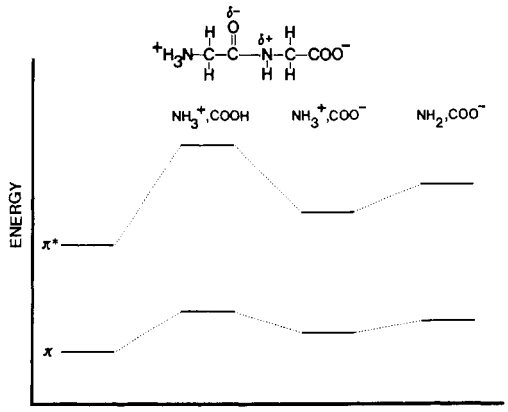

Figure 12. Energy level perturbation for the amide π and π^* electronic states due to inductive effects from the terminal groups.

sections. We assumed that the oscillator strengths were proportional to the product of the maximum molar absorptivity times the absorption band half-width on the long-wavelength side.

The increase in molar absorptivity and λ_{max} values probably derives from deprotonation of the terminal carboxylate group which forms the zwitterion.[55] The observed absorption spectral changes due to zwitterion formation for the amide group are greater than the absorption difference that occurs between a carboxyl group and a carboxylate anion.

About 20% of a π electron is transferred from the nitrogen atom to the carbonyl group in the ground electronic state of the amide linkage. The $\pi \rightarrow \pi^*$ excitation transfers between 40 and 73% of a π electron from the nitrogen to the carbonyl group.[38] Thus, the amide π^* excited electronic state has more ionic character than the ground state. The energies of the amide ground and excited states are perturbed by the ionic character and electron-donating and -withdrawing nature of the amide substituents.[38] Figure 12 shows a qualitative energy level diagram that depicts the energy perturbation resulting from the inductive effect of the end-group substituents. An electron-withdrawing substituent attached to the amide nitrogen will increase the energies of both ground and excited states, in proportion to the strength of the inductive effect and its effect upon decreasing the electron density at the nitrogen. Because the excited state is more ionic than the ground state, the excited-state energy will be increased more than the ground state. Thus, the electron-withdrawing COOH substituent will increase the energy of the excited state more than the ground state. Since COO^- is less electron withdrawing, it increases the excited- and ground-state energies less than does COOH. Thus, the transition energy gap between the ground and excited electronic states will be larger for COOH than for COO^-. In contrast, an electron-withdrawing group attached to the carbonyl carbon of the amide linkage stabilizes the ionic character of both ground and excited states. Since an NH_3^+ is more electron withdrawing than NH_2, NH_3^+ stabilizes the electronic ground and excited states of the $\pi \rightarrow \pi^*$ transition relative to NH_2. Therefore, COO^- and NH_3^+ terminal groups decrease the transition frequency of the system compared to the COOH and NH_2. As the pH is altered, the protonation states of the terminal groups titrate between the COOH and COO^- and NH_3^+ and NH_2 charged forms. As Figure 12 shows, the lowest frequency transition occurs for the zwitterion ^+H_3N---COO^-. Thus, we expect a maximum preresonance enhancement for our 218-nm excitation at ca. pH = 4.5, where the zwitterionic concentration is a maximum.

The oscillator strength also depends upon pH. We expect a maximum oscillator strength for the zwitterion $\pi \rightarrow \pi^*$ transition due to interactions between the transition moment of the amide $\pi \rightarrow \pi^*$ transition with the zwitterion dipole. The transition moment of the amide $\pi \rightarrow \pi^*$ transition lies in the direction indicated in Figure 13 at angle of 9.1° to the N–O axis.[37,53] The transition dipole moment is oriented approximately opposite to the direction of the zwitterion permanent dipole moment. This will result in hyperchromism for the $\pi \rightarrow \pi^*$ absorption band due

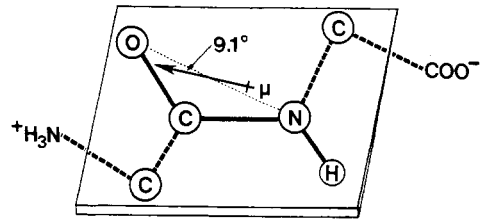

Figure 13. Diagram showing the direction of the transition moment of the amide $\pi \rightarrow \pi^*$ transition (from ref 37 and 53).

to an increased transition moment for the zwitterion due to end-group inductive effects and an increased conjugation. The maximum oscillator strength will occur at the maximum zwitterion concentration at ca. pH = 4.5.

Secondary Structure Determinations in Proteins. We can use the experimentally observed amide differential Raman cross sections to determine peptide and protein secondary structure. The differential Raman cross sections are the experimentally observed values of the Raman cross section (cm^2/(amide linkage·sr)) at each frequency within a Raman spectrum, ν. Total Raman cross sections which are also often reported are integrated Raman cross sections (it should be noted, however, that the total Raman cross sections for bands narrower than the instrument resolution are equal to the maximum differential Raman cross sections).

We can use spectra such as those shown in Figures 2 and 3 (after correction for instrument throughput) to model protein and peptide secondary structure from the relationship

$$S(\nu,\nu_0) = \chi_\alpha\sigma_\alpha(\nu,\nu_0) + \chi_\beta\sigma_\beta(\nu,\nu_0) + \chi_r\sigma_r(\nu,\nu_0) + C(\nu,\nu_0) + D(\nu,\nu_0) \quad (4)$$

The observed Raman spectrum $S(\nu,\nu_0)$ excited at ν_0 is made up of contributions from the α-helix, β-sheet, and random coil conformations. We can model the amide Raman spectral region of a protein by summing the product of the mole fraction, χ_i, times the differential Raman cross section, $\sigma_i(\nu,\nu_0)$, for each conformation. In a protein we expect overlap from the Raman scattering of the amino acid side chains, and the extent of overlap will be different for each protein and given by the parameter $C(\nu,\nu_0)$. To simplify our analysis, we constrain our system such that the sum of mole fractions is equal to 1:

$$\chi_\alpha + \chi_\beta + \chi_r = 1 \quad (5)$$

Thus, we include the phenomenological parameter $D(\nu,\nu_0)$, which accounts for the fact that amide linkage conformations may also exist in strained configurations different than those typically occurring in the α-helix, β-sheet, and random coil forms. In this model $D(\nu,\nu_0)$ may be either positive or negative since the mole fraction sum is artificially constrained to be equal to 1 and since the relative amide intensities may be dramatically different from those for the α-helix, β-sheet, or random coil conformations.

Ultimately, the most reliable secondary structure determination will derive from differential Raman cross section spectral curve fitting. This will require extensive characterization of aromatic amino acid Raman cross sections. Indeed, the aromatic amino acids dominate the intensities observed at 218 nm, and it is certain that the amide modes are best studied with excitation at shorter wavelengths such as at 200 nm. Indeed, our work here allows us to now assign the clearly observed but previously misassigned ca. 1400-cm^{-1} band in α-lactalbumin,[16] cytochrome c,[17] and tropomyosin[13] to the amide 2V band. This band is clearly isolated and strong in these previously reported far-UV excited Raman spectra. We are in the process of characterizing the cross sections of the amide bands and the aromatic amino acids in the 200-nm spectral region. However, we can demonstrate the strong secondary structure dependence of the cross section of the amide 2V band frequency by plotting the intensity of the amide 2V band of tropomyosin as obtained from literature spectra against the reported α-helical content.

Tropomyosin has only α-helix and random coil forms, and the relative abundance of each depends upon the solution pH. The

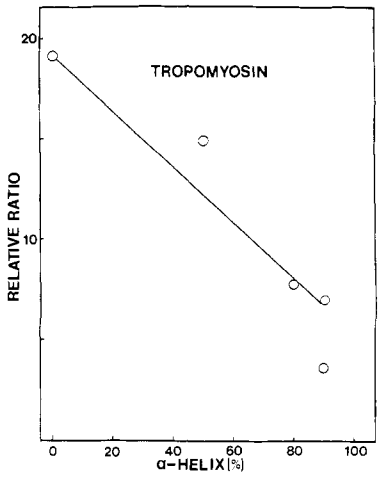

Figure 14. Dependence of the relative intensity of the amide V overtone band on α-helix content of rabbit muscle tropomyosin (from spectra of ref 13).

published[13] 200-nm excited Raman spectra at different pH values show the amide 2V band at 1395 cm^{-1} as well as the 981 cm^{-1} SO_4^{2-} internal standard band. Figure 14 shows the relative ratio of the amide 2V intensity as a function of α-helical content. The linear correlation indicates that, as expected, the amide 2V band intensity is a good monitor of secondary structure. Indeed, the correlations we observe for the amide 2V band are similar to those earlier observed in this same tropomyosin study for the amide II and III bands.[13]

We can begin analysis of protein secondary structure even prior to determining the differential Raman cross sections of all amino acid side chains. While not as accurate, we can develop simple relationships to determine the relative abundance of the α-helix, β-sheet, and random coil forms. Since we have three unknowns, we require at least three robust equations. Given our constraint on the mole fractions (eq 5), we require two independent measurements of the differential Raman cross sections. Obviously, the amide 2V intensities for the random coil and β-sheet conformations are easily measured since they occur in a spectral region with little overlap from the aromatic amino acids. In fact, the most sensitive measure is the maximum differential Raman cross section between 1380 and 1400 cm^{-1} of the amide 2V band because it differs most dramatically between the different forms:

$$S^{2V}(\nu_0) = \chi_\alpha \sigma_\alpha{}^{2V}(\nu_0) + \chi_\beta \sigma_\beta{}^{2V}(\nu_0) + \chi_r \sigma_r{}^{2V}(\nu_0) \qquad (6)$$

where we assume $C(\nu,\nu_0)$ is negligible and for the moment assume $D(\nu,\nu_0) = 0$. The 1400-cm^{-1} differential Raman cross sections for 218-nm excitation for the amide 2V band are as follows: α-helix, 0.96; β-sheet, 8.27; random coil, 5.97.

The most sensitive other expression that utilizes the largest cross-section differences between the conformations utilizes the cross sections of the amide II bands is

$$S^{II}(\nu_0) = \chi_\alpha \sigma_\alpha{}^{II}(\nu_0) + \chi_\beta \sigma_\beta{}^{II}(\nu_0) + \chi_r \sigma_r{}^{II}(\nu_0) \qquad (7)$$

Although this band is strongly overlapped by tryptophan, it should be easy to accurately numerically remove the tryptophan contribution by examining the tryptophan intensity at 1000 and 757 cm^{-1}; the dispersions of the cross sections for these three bands are very similar.[9] Thus, we can determine the amide II cross sections in proteins by subtracting the tryptophan contribution.

As an example of this type of analysis, we have determined the relative abundances of the conformations of PLL at different pH values from the spectra shown in Figure 6. Using the amide II cross sections of Table II and the values for amide 2V discussed above, we conclude that Figure 6A (pH = 10.6, 0 °C) contains 100% α-helix. Figure 6B (pH = 10.6, 52 °C) contains 55% α-helix and 41% random coil and negligible β-sheet. Figure 6C (pH = 10.8, 52 °C) is 83% α-helix and 20% random coil with negligible β-sheet. A transition begins to be apparent in Figure 6D (pH = 11, 52 °C) which is 82% α-helix and 25% β-sheet while Figure 6E (pH = 11.3, 52 °C) is 100% β-sheet. Thus, we can quantitatively monitor transitions in peptide secondary structure. We have constrained the sum of the mole fractions to be 1, and thus these simple expressions can calculate small negative coefficients for minor conformations. Indeed, these calculations indicate that the maximum α-helical content occurs at pH = 10.8 with a simultaneous minimum in the β-sheet conformation (Figure 6C). In agreement, the pH = 10.8 spectrum showed a minimum in the Raman cross sections as plotted in Figure 7. We conclude that the simple relationships proposed here will be generally useful for protein secondary structure determinations, especially at shorter wavelength excitations.

Conclusions

The results reported here describe the conformational and ionization dependences of the amide band UV Raman frequencies and cross sections. The strong conformational frequency and Raman cross section dependences of the amide bands indicate that they are useful sensitive monitors of protein secondary structure. By exciting the amide bands below 210 nm, we can selectively study secondary structure. In contrast, excitation between 210 and 240 nm selectively enhances aromatic amino acid bands to permit the investigation of tyrosine and tryptophan environment. This independent and distinct spectral information can be combined to detail protein structure at different geometric sites. The results reported here will be used in Future UV Raman studies of proteins.

Acknowledgment. We gratefully acknowledge helpful conversation with Professor Sam Krimm and further acknowledge support of this work from NIH Grant 1R01GM30741-07. S.A.A. is an Established Investigator of the American Heart Association. This work was done during the tenure of an Established Investigatorship of the American Heart Association, Pennsylvania affiliate.

Registry No. PGA·Na (homopolymer), 26247-79-0; PGA·Na (SRU), 28829-38-1; PLL·HCl (homopolymer), 26124-78-7; PLL·HCl (SRU), 28575-12-4; DGL, 556-50-3; TGL, 556-33-2; AGL, 543-24-8; DLA, 1948-31-8; DLV, 3918-94-3; DLL, 13184-13-9; DLG, 3929-61-1; GA, 106-57-0.